Computational and Theoretical Chemistry 1239 (2024) 114792

Contents lists available at ScienceDirect

Computational and Theoretical Chemistry

journal homepage: www.elsevier.com/locate/comptc

Prediction study of Optical, structural and electronic properties of WCl*x* (*x* = 3 to 6)

R. Boudissa [a], Y. Madkour [a], T. Chihi [b], M.A. Ghebouli [b,c], H. Bouandas [d], F. Benlakhdar [b], M. Fatmi [b,*], B. Ghebouli [a], Munirah D. Albaqami [e], Saikh Mohammad [e], M. Habila [e], M. Sillanpää [f,g,h]

[a] *Laboratory for the Study of Surfaces and Interfaces of Solid Materials (LESIMS), University Ferhat Abbas of Setif 1, Setif 19000, Algeria*
[b] *Research Unit On Emerging Materials (RUEM), University Ferhat Abbas of Setif 1, Setif 19000, Algeria*
[c] *Department of Chemistry, Faculty of Sciences, University of Mohamed Boudiaf, M'sila, 28000, Algeria*
[d] *Applied Optics Laboratory, Institute of Optics and Precision Mechanics, University Ferhat Abbas Setif 1, Setif 19000, Algeria*
[e] *Department of Chemistry, College of Science, King Saud University, P.O. Box 2455, Riyadh 11451, Saudi Arabia*
[f] *Department of Biological and Chemical Engineering, Aarhus University, Norrebrogade 44, 8000 Aarhus C, Denmark*
[g] *School of Technology, Woxsen University, Hyderabad, Telangana, India*
[h] *Department of Chemical Engineering, School of Mining, Metallurgy and Chemical Engineering, Uni-versity of Johannesburg, P. O. Box 17011, Doornfontein 2028, South Africa*

A R T I C L E I N F O

Keywords:
Molecular structure
CASTEP
Tungsten chloride
Band structure
GGA-PBESOL

A B S T R A C T

The molecular structures of WCl_6, WCl_5, WCl_4, WCl_3 have been optimized by density functional theory calculations. We report the stability of the phases in the ground state, the total energies and the optoelectronic properties of the W-Cl system. We find that the material having a low tungsten concentration shows a low DOS at the Fermi level, which implies a high resistivity. Both polymorphs of WCl_6 are crystalline solids at room temperature and show the (α- WCl_6) and (β- WCl_6) phases of space group *R*-3 and *P*-3 m1 observed at 228 °C. The change in temperature influences the structural, electronic and optical properties. The object of this paper does not concern only the study of all phases, but also one controls the physical states of the molecular materials when they are subjected to polymorphic changes. Calculations on the molecular structure under symmetry indicated an orbitally degenerate ground state with bond distances in good agreement with experiment.

1. Introduction

Tungsten hexachloride is a chemical compound containing tungsten and chlorine with the stoichiometric formula WCl_6. It is used as the cathode in chloride-ion batteries, which are a new and emerging battery technology that provide high theoretical volumetric capacity at low cost [1]. The study of the phase diagram of the W-Cl system carried out by H. Okamoto [2] is illustrated in Fig. 1. The phase diagram is presented to show the effect of temperature and concentration on the present phases structure of the alloy at constant pressure, where an equilibrium state corresponds to the minimum value of free energy. The study of the phase diagram helps to clarify the phase transformations produced during processing under heating conditions. We note that the optimized tetrahedral structures WCl_6, WCl_5 and WCl_4, the planar trigonal structure WCl_3 and the molecular structure W_2Cl_6 were studied by Bernd Schimmel Pfennig et al. using the quasi-relativistic potential for the electrons core [3]. Fluorescence called photoluminescence is defined as the excitation caused by the absorption of a photon, where the electronic transition responsible for fluorescence does not change the spin of the electrons, resulting in short-lived electrons in the state excited in the W-Cl system. The interest in the study of W-Cl alloys is very important because of their interesting mechanical parameters and their technological importance, notably engineering, electronics and mechanics. Indeed, it is reported that V. Sliznev and N. Belova studied the Jahn-Teller effect and the spin–orbit coupling of the compound MX_3 and MX_4 (M=Mo, W and X =F, Cl) [4]. We present the atomic and weight percent chlorine in the range 80 to 86 and 44 to 53 under temperature effect between 140 ^{0}C and 300 ^{0}C. The phases which appear in Fig. 1 are WCl_3, αWCl_5, βWCl_5, αWCl_6, βWCl_6, and γWCl_6.

Other research carried out by Andrew Sevy et al. provide the first

* Corresponding author.
E-mail address: fatmimessaoud@yahoo.fr (M. Fatmi).

https://doi.org/10.1016/j.comptc.2024.114792
Received 3 May 2024; Received in revised form 14 July 2024; Accepted 26 July 2024
Available online 29 July 2024

measurement of the bond energies of the WCl molecule [5]. Uncertainty is reported to remain in WClx alloys rich in W due to their stable crystal phases. Tungsten has a melting point of 3680 °C, hence its use in high temperature applications such as aerospace and arc welding processes. Tungsten also is a transition metal that exists in equilibrium in two polymorphic forms such as the more stable β-W cubic structure (*Im*-3 m, No 229) and the metastable α-W cubic structure (*Pm*-3*n*, No 223). Chlorine is a bimolecular gas Cl_2, which is used in the manufacture of consumer products, such as polyvinyl chloride and the production of plastics. The first crystal structure of solid chlorine synthesized at room temperature and a pressure of 1.45 GPa [6] and extracted from a powder and X-ray diffraction shows the tetragonal symmetry [7]. A detailed study of the single crystal Cl_2 by X-ray diffraction reveals an orthorhombic structure of iodine and the bromine Cmca [8]. limited amounts of alkyl halides produced from the combination of WCl_6 with some other *N*-aryl α-demines [9] were detected. We optimized by the density functional theory with a quasi-relativistic potential the molecular structures WCl_6, WCl_5, WCl_4, WCl_3 and the dimer W_2Cl_6. The tri- and dichlorides reveal the presence of W_2Cl_6, WCl_5, and WCl_4 species in the gas phase, but no measurable levels of monomeric WCl_3 or WCl_2 [10]. WCl_6 is used in the preparation of catalysts to obtain a coating of tungsten on a substrate to improve electrical conductivity in windows and windshields [11,12]. Tungsten chloride with a melting point of 282 °C is absorbed through the respiratory and digestive tract [13]. Cl/O interchange took place when WCl_6 was allowed to interact with a series of α-amino-acids [14]. B. Marco et *al.* [15] studied the reaction of WCl_6 with a selection of carboxylic acids using dichloromethane as reaction medium. The production of WCl_6 is obtained by chlorination of metallic tungsten at temperature 600 °C, as indicated by the following relation:

$$W(s) + 3Cl_2 \rightarrow WCl_6$$

The WCl_6 reaction product has a blue-black crystalline solid at room temperature and takes (α-WCl_6) and (β-WCl_6) phases with approximately 56 % (α-WCl_6) and 44 %(β-WCl_6). J.C. Taylor et al. studied the (β-W) hexachloride structure by neutron powder and X-ray diffraction [16]. Deane K. Smith et *al.* [17] synthesize and suggest that the crystal structure of WCl_6 is isostructural and exhibits a polymorph β-WCl_6. The second polymorph is α-WCl_6 of hexagonal structure with lattice parameters $a = 6.088$ Å and c = 16.68 Å and space group *R*-3. Inorganic pentachloride tungsten WCl_5 is prepared by reduction of tungsten hexachloride and exists as a dimer. Cotton et *al.* [18] have been studied the WCl_5 compound in the monoclinic crystal structure. WCl_4 is synthesized from WCl_6 by reducing WCl_6 with Al [19,20] according to the equation:

$$3WCl_6 + 2Al \rightarrow 3WCl_4 + 2AlCl_3$$

WCl_4 has a monoclinic crystal structure with space group *C*2/*m*, *Z*=4 and lattice parameters $a = 11.782$ Å, $b = 6.475$ Å, $c = 8.062$ Å, β = 131.14°. Inorganic tungsten WCl_3 is a brown solid obtained by chlorination of tungsten chloride [21]. The aim of this work is the study of the structure and lattice parameters, the stability, the electronic and optical parameters of the trigonal (*R*-3, 148) WCl_3, monoclinic (*C*2/*m*, 12) WCl_4, monoclinic (*C*2/*m*, 12) WCl_5, hexagonal (*P*-3 m1, 164) β-WCl_6 and hexagonal (*R*-3, 148) α-WCl_6. The scope of this study explains the extent to which the research area will be explored and specifies the parameters within this study will be operating.

2. Calculation models

We use the CASTEP code in the calculation of crystal structure and optoelectronic properties for WCl_x ($x = 3$ to 6) [22]. Schrödinger's equations were solved according to the formalism of density functional theory. During the calculations, we use the norm-conserving pseudo potential of GGA-PBESOL [23] to characterize the valence electrons. We choose a cut_{off} energy of 300 eV and 4x4x4 Monkhorst-Pack grid to perform reciprocal space [24]. The optimization of W, WCl_x($x = 3$ to 6) and Cl_2 was done by GGA-PBESOL and LDA [25–27]. The Broyden-Fletcher-Goldfarb technique was used to calculate the equilibrium lattice parameters. The fastest technique to identify the lowest energy structure is typically provided by this strategy. The tolerance of the self-consistency calculation is 2.10^{-5} eV/atom. We adopt the following convergence thresholds, such as total energy change smaller than 2.10^{-5} eV/atom, maximum force per atom below 0.05 eV/atom, pressure smaller than 0.1 GPa, and maximum atomic displacement below 2×10^{-3} Å. The electrons of an atom are divided into valence and core electrons. Valence electrons occupy the outermost shell (highest energy level) of an atom, while core electrons are those occupying the innermost shell (lowest energy levels). Valence electrons participate in the formation of chemical bonding, while core electrons influence the chemical reactivity of an atom. The electronic configuration of W and Cl are noticed as W: [Xe] $4f^{14}$ $5d^4$ 6 s^2 and Cl: [Ne] 3 s^2 $3p^5$.

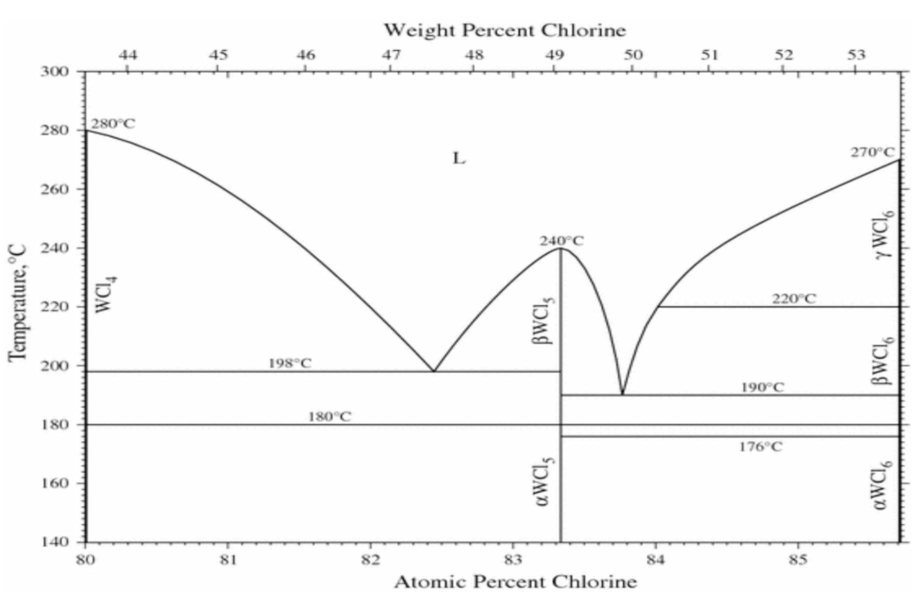

Fig. 1. The region 80 to 86 atomic Cl % of the phase diagram for the W-Cl system [2].

3. Results and discussions

3.1. Structural parameters

We collect in Table 1, all information about crystal structure, space group, lattice parameters, β angles, volume and number of cells, which agree well with experimental values [6,8,16,17,20,28,29]. We studied the Cl_2 orthorhombic structure (Cmca, 64) at 0 GPa and 1.45 GPa. It is noted that the pressure reduces the lattice parameters and volume, where the results agree reasonably with experimental ones [6,8]. We show in Table 2 the total energy, density and bond lengths between atoms for all compounds. We noticed that there are several bonds Cl-W and W-W with lengths within 2.3941 to 2.4656 (\AA) range. Fig. 2; shows the effect of Cl content on optimization energy for W-Cl system and explains the structural stability of these materials. The degree of stability in these molecules follows the following sequence $WCl_5 \rightarrow WCl_3 \rightarrow$ α-$WCl_6 \rightarrow$ β-WCl_6. The monoclinic WCl_5 (*C2/m*, 12) and the trigonal WCl_3 (*R*-3, 148) are the more stable phases. The bonds lengths of W, WCl_3, WCl_4, WCl_5 and $2Cl_2$ are in well agreement with experimental values reported in the literature [8,10]. Fig. 3 represents a view of the (001) plane and perspective view of WCl_3, WCl_4, WCl_5, β-WCl_6 and α-WCl_6.

Our study confirms that WCl_5 and WCl_3 are the compounds the more stable. The total minimum energy of W, WCl_3, WCl_4, WCl_5 WCl_6 and $2Cl_2$, in their ground state phases lay on a common straight line. This straight line implies that the concentration range of the different compounds is quite narrow and that the phase diagram consists mainly of two-phase regions. The ground state of WCl_4 is a tetrahedral triplet (Td), while that of WCl_3 is a trigonal planar quartet (D3h). WCl_6 phase may be present in two crystal forms, such as β-WCl_6 hexagonal (*P*-3 m1, 164) and α-WCl_6 hexagonal (*R*-3, 148). The W atoms in β-WCl_6 lie in octahedral holes in the hexagonal close-packed chlorine, and the octahedra around (W) are nearly regular. Six Cl atoms surround each W atom. Fig. 3 shows a view of the projection of the atomic positions in the plane (001) and a perspective view for WCl_3, WCl_4, WCl_5, β-WCl_6 and α-WCl_6. The mean W-Cl bond distance found in the crystalline phase 226 (2) pm [16], although less accurate, is in good agreement with the gas phase value. The bond distance in α-WCl_6 (β-WCl_6) obtained in this study is 2.321 Å (2.30646 Å to 2.34198 Å) appears to be significantly longer than the mean bond distances in WCl_4 and WCl_5 (2.234 Å) and (2.265–2.568 Å) respectively. The mean bond distances in WCl_4 and WCl_5 calculated by other researchers are 2.248 Å and 2.26 Å [30,31] respectively. As a result, shorter bonds are stronger, because strength is inversely proportional to length. A more stable and shorter bond will be more difficult to break. WCl_5 phase follows the stacking sequence ABAC with W atoms and W vacancies in the holes. For each of these considered compounds, except for α-WCl_6 case, the lowest energy structure is found to have the highest $N(E_f)$ value, where no experimental value is available for comparison. The total density of states at the Fermi level at T=0°K for WCl_4 is 3.272 states per eV and per atom. The corresponding band structures of these materials are a semi-conductor with a band gap of 1.746 eV and

Table 2
Total energy, density and bond lengths between atoms for W, WCl_3, WCl_4, WCl_5, β-WCl_6, α-WCl_6 and Cl_2.

Compounds	Energy (eV)	Density	Bond length (Å)
W	−1699.4328	19.1483	W-W: 2.517
WCl_3	−25742.4449	4.7524	W-Cl: 2.3941–2.4656
			2.246 [8]
WCl_4	−7323.6618	2.79290	W-Cl: 2.234
			2.265 [8]
WCl_5	−26903.3298	3.40460	W-Cl: 2.265–2.568
		3.86 [3]	2.273 [10]
β-WCl_6	−7943.9795	2.54024	W-Cl: 2.316–2.342
			2.321 [10]
α-WCl_6	−7951.9897	3.35984	W-Cl: 2.321

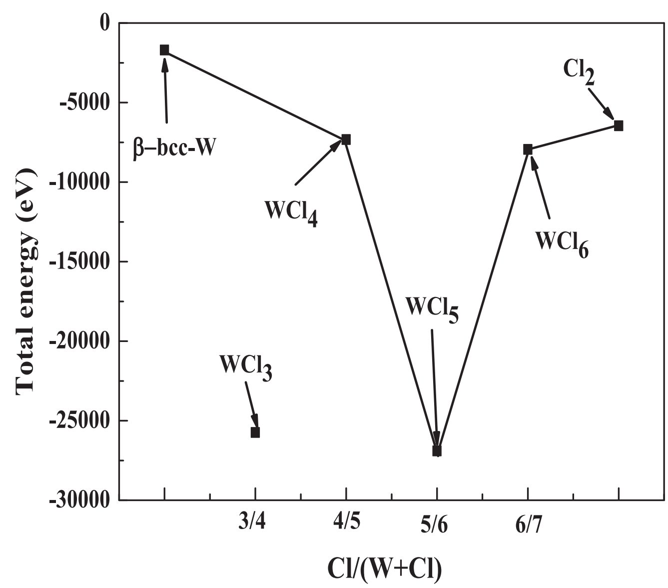

Fig. 2. The effect of Cl content on total energies of W-Cl system.

Table 1
Space groups, lattice parameters, angle, conventional volume, number of cell formula of compounds and reference in the W-Cl system. (a) This study at 0 GPa, (b) This study at 1.45 GPa.

Structure	a_0 (Å)	b_0 (Å)	c_0 (Å)	β (°)	V_0 (Å^3)	Z	References
β-W_8 (cubic, *Pm*-3*n*, 223)	5.0331	–	–	–	127.548	1	This study
	5.0460	–	–	–	128.481		[31]
WCl_3 trigonal	15.6815	15.6815	8.5703	–	1825.21	18	This study
(*R*-3, 148)	14.9352	14.9352	8.4553	–	–		[32]
WCl_4 monoclinic	15.1306	6.3668	9.2245	119.38	774.498	4	This study
(*C2/m*, 12)	11.782	6.475	8.062	131.14	463.20		[20]
WCl_5 monoclinic	18.0385	18.4810	6. 3661	95.20	2113.54	12	This study
(*C2/m*, 12)	17.438	17.706	6.063	95.51	1863.36	12	[18]
β-WCl_6 hexagonal	11.8459	–	6.3994	–	777.702	3	This study
(*P*-3 m1, 164)	10.493	–	5.725	–	–		[1617]
	10.511		5.757		–		
α-WCl_6 hexagonal	6.3649	–-	16.7591	–-	587.989	3	This study
(*R*-3, 148)	6.088	––	16.68		–––	3	[16]
Cl_2 orthorhombic	8.5790	5.0377	8.8041	–	380.503	4	This study (a)This study
(Cmca, 64)	6.9445	4.2778	8.2451	–	244.944	4	(b)
	5.9988	4.3231	7.9919	–	207.220	4	[68]
	6.29	4.50	8.21	–	–––	4	

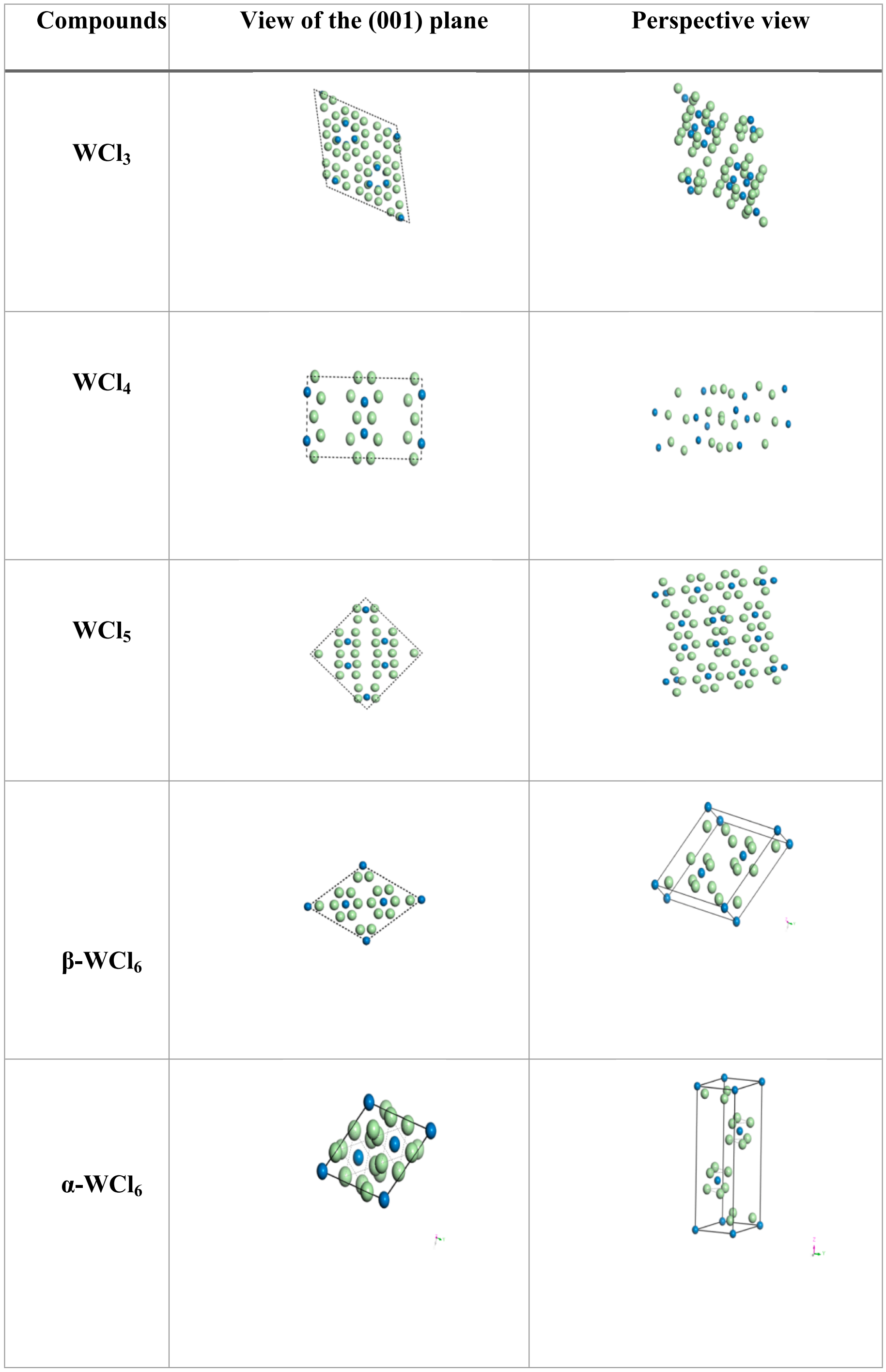

Fig. 3. The view of the (0 0 1) plane and perspective view of WCl_3, WCl_4, WCl_5, β-WCl_6 and α-WCl_6.

1.806 eV, which is conform to available experimental value 1.917 eV [32]. Fig. 4 shows the energy as a function on volume for WCl_3 (a), WCl_4 (b), WCl_5 (c), β-WCl_6 (d) and α-WCl_6 (e). All energies are negative, then all these alloys are stable.

3.2. Electronic band structure

We will discuss the electronic band structure and the projected density of state (PDOS) of materials. We show in Fig. 5 the band structures and total densities of states of β-WCl_6, α-WCl_6 and WCl_5 performed with GGA- PBESOL. The lowest energy of conduction band is at Γ point, while the highest energy of valence band is at Γ point, which indicate a direct Γ-Γ band gap for WCl_3, WCl_5, β-WCl_6 and α-WCl_6 (1.78 eV, 0.08 eV, 1.746 eV and 1.803 eV), while WCl_4 has the metallic character. The over lapping of the bands and the existence of a density of state in the DOS at the Fermi level are the signs that WCl_4 shows a metallic character. We note that DOS curves of WCl_3, WCl_5, β-WCl_6 and α-WCl_6 and band structure are consistent. The atomic geometry of monoclinic WCl_4 and WCl_5 contain an ordered arrangement of W vacancies.

The common features in the PDOS profile for the studied compounds consist in the fact that W and Cl have a similar profile throughout the whole energy region, indicating the presence of hybridization between W and Cl sites. The contribution at the upper valence band is mainly the W-3d and Cl-3p states. The sharp peaks correspond to maximum

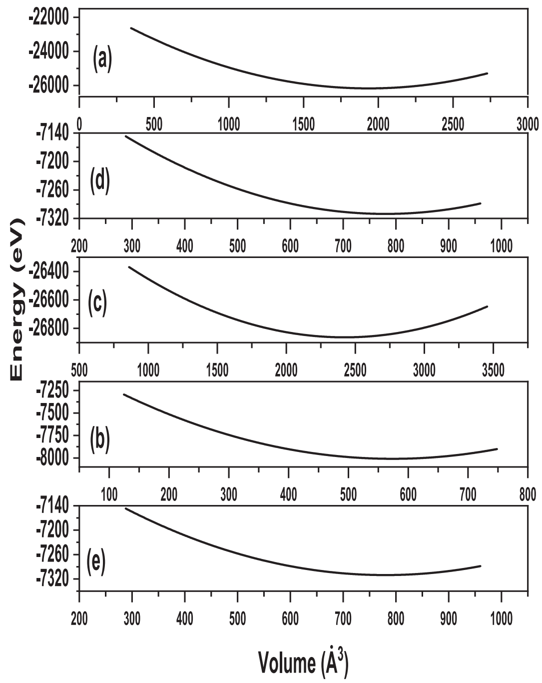

Fig. 4. Energy as a function on volume of WCl_3 (a), WCl_4 (b), WCl_5 (c), β-WCl_6 (d) and α-WCl_6 (e).

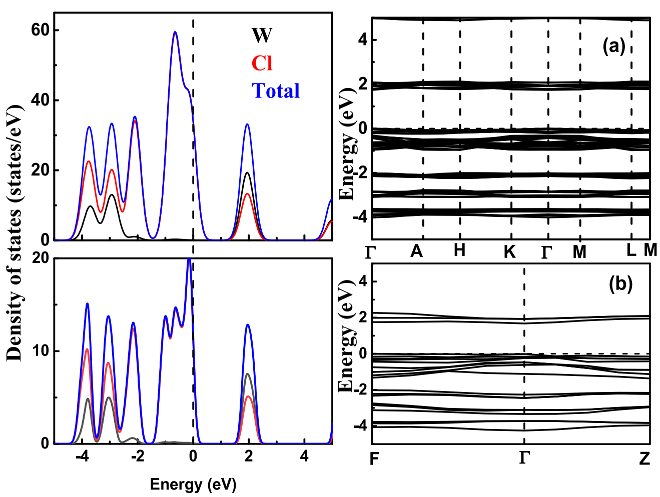

Fig. 5. Band structures and total densities of states of β-WCl_6 (a) and α-WCl_6 (b).

electronic contributions for distinct energies, while in a plateau the electronic contribution is almost identical in an energy range. Hirshfeld charges are due to the strain density, which is the difference between the molecular and unrelaxed atomic charge densities. The quantitative description of charge distributions in a molecule requires dividing a system into atomic fragments. A general and natural choice is to share the charge density at each point between the atoms, in proportion to their free-atom densities at the corresponding distances from the nuclei. This prescription yields well-localized bonded-atom distributions each of which closely resembles the molecular density in its vicinity. Integration of the atomic deformation densities bonded minus free atoms defines the net atomic charges and multipole moments which concisely summarize the molecular charge reorganization. This permits calculation of the external electrostatic potential and the interaction energy between molecules or between parts of the same molecule. Mulliken populations analysis of WCl_x ($x = 3$ to 6) compounds allows the evolution description of charge transfers and binding interactions in molecular systems. We report in Table 3 the lengths and overlap populations of the shortest atomic bonds W-W, Cl-Cl and Cl-W in WCl_3, WCl_4, WCl_5, α-WCl_6 and β-WCl_6 compounds and some experimental values [6,10,20,32]. The mean interatomic distances are in total agreement with those given experimentally for either α-WCl_6 or β-WCl_6, which the DFT is a good calculation tool. We display in Table 4 the partial atomic charges (Mulliken populations) in the different atoms for WCl_3, WCl_4, WCl_5, β-WCl_6 and α-WCl_6. The atomic charges given by the calculations follow the expected chemical trends and are also similar to the Hirshfeld atomic charges.

3.3. Optical properties

The reflectivity, absorption, loss function, conductivity, dielectric function, refractive index and extinction coefficient were calculated for β-WCl_6, α-WCl_6 and WCl_5. These parameters are anisotropic for materials in the hexagonal structure. We report in Figs. 6-8; the effect of photon energy on reflectivity, absorption, conductivity, real and imaginary parts of dielectric function, refractive index and loss function for β-WCl_6, α-WCl_6 and WCl_5. The reflectivity is a measure of the ability of a material to reflect radiation. The static reflectivity of β-WCl_6, α-WCl_6 and WCl_5 is 0.07, 0.04 and 0.16 and reaches several peaks of maxima in the field of extreme ultraviolet light. The maximum reflectivity of about 20 %, 22 % and 100 % is obtained at 20 eV, 5 eV and 20 eV for β-WCl_6, α-WCl_6 and WCl_5. These materials are reported to absorb ultraviolet light in the range 5 eV to 20 eV. This improvement validates the candidature of β-WCl_6, α-WCl_6 and WCl_5 materials for optical and photovoltaic devices. The maximum absorption coefficient of about 25.10^4 cm^{-1}, 17. 10^4 cm^{-1} and 35. 10^4 cm^{-1} is obtained at 16 eV for β-WCl_6, α-WCl_6 and WCl_5. β-WCl_6, α-WCl_6 and WCl_5 materials do not undergo strong delocalization (number of double bonds $\geq$ 10), then absorption does not occur in the visible region. The absorption capacity is explained by the imaginary part of the dielectric function. The intense peak of the imaginary part of β-WCl_6, α-WCl_6 and WCl_5 is located at a photon energy of 5 eV. The absorption is produced in the extreme ultraviolet range. Small peaks are noticed in the ultraviolet range. The features of the energy-loss spectra are related to the photonic band structure of the crystal. The interaction of electrons with the crystal contributes to the energy loss. The electron energy loss of 7 %, 22.5 % and 8 % for β-WCl_6, α-WCl_6 and WCl_5 alloys are localized in the ultraviolet light region (20 eV). We represent the effect of photon energy on real and imaginary parts of optical conductivity. The static conductivity of β-WCl_6, α-WCl_6 and WCl_5 is 1.7 Ω^{-1}cm^{-1}, 1.5 Ω^{-1}cm^{-1} and 2.3 Ω^{-1}cm^{-1}. The appearance of the three conductivity spectra in the energy range 5 and 20 is identical. The flat in the conductivity spectrum

Table 3
Bonds, populations of all electron configurations and length of WCl_3, WCl_4, WCl_5, β-WCl_6 and α-WCl_6.

Compound	Bonds	Population	Length (\AA)
WCl_3	Cl – W	0.35 to 0.54	2.3941 to 2.4656
			2.376 to 2.418 [32]
	W – W	0.07 to 0.11	2.92739 to 2.93765
			2.869 to 2.879 [32]
WCl_4	Cl –W	0.04 to 0.68	1.83947 to 2.96164
		0.54 [20]	2.280 to 2.5 [20]
			2.265 [10]
WCl_5	W – W	0.94	2.49389
	Cl –W	0.31 to 0.60	2.284 to 2.56804
β-WCl_6	Cl –W	0.54	2.30646 to 2.34198
			2.321
			2.24 [6]
α-WCl_6	Cl – W	. 0.53	2. 0.321
	Cl – Cl		2. 2.24 [6]
			3.27703

Table 4
Specie, partial atomic charges (Mulliken populations), charge and Hirshfeld charge (e) in the different atoms for WCl_3, WCl_4, WCl_5, β-WCl_6 and α-WCl_6.

	Specie	s-Orbitals (e)	p-Orbitals (e)	d-orbitals (e)	Total (e)	Charge (e)	Hirshfeld charge (e)
WCl_3	Cl	1.95	5.14 to 5.40	0.00	7.09 to 7.34	−0.09 to −0.34	−0.21 to 0.04
	W	0.55	0.33	4.6	5.48	0.52	0.15
WCl_4	Cl	1.93 to 1.95	5.06 to 5.27	0.00	6.99 to 7.22	−0.22 to 0.01	−0.08 to 0.01
	W	0.85	0.15	4.55	5.56	0.44	0.16
WCl_5	Cl	1.94 to 1.95	5.22 to 5.30	0.00	7.17 to 7.24	−0.17 to −0.24	−0.09 to 0.06
	W	1.95	0.29	4.36 to 4.37	5.07 to 5.08	0.92 to 0.93	0.35
β-WCl_6	Cl	1.95	5.22	0	7.17	−0.17	−0.07
	W	0.36 to 0.39	0.27 to 0.39	4.27 to 4.31	4.95 to 4.96	1.04 to 1.05	0.43 to 0.44
α-WCl_6	Cl	1.95	5.22	0	7.17	−0.17	−0.07
	W	0.39	0.31	4.29	4.98	1.02	0.44

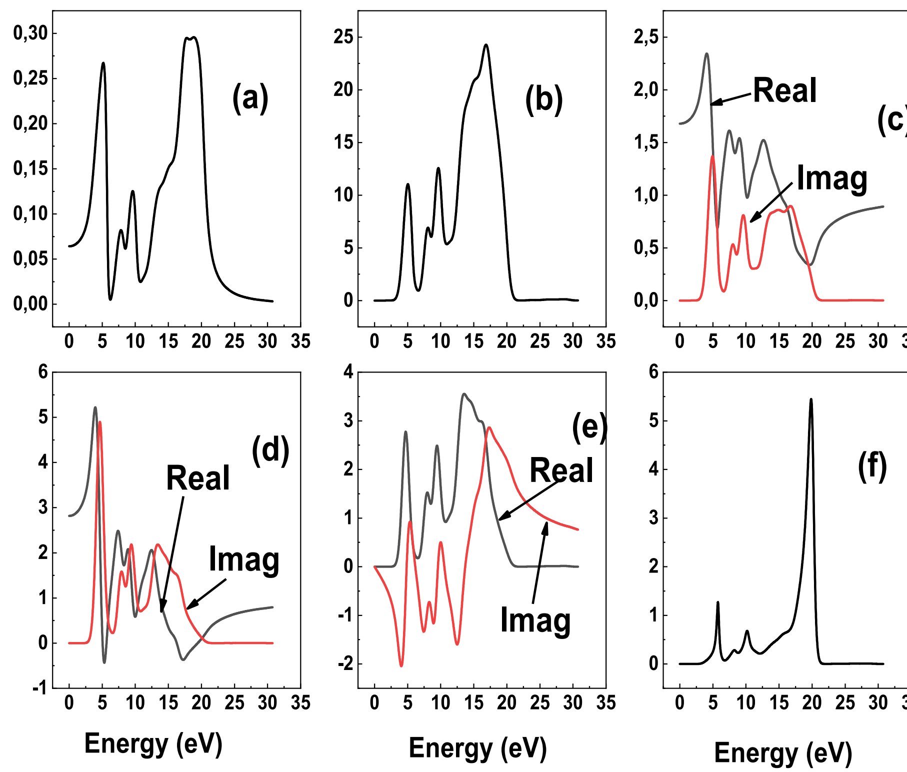

Fig. 6. The reflectivity (a), absorption (10^4 cm^{-1}) (b), conductivity (c), real and imaginary parts of dielectric function (d), refractive index (e) and loss function (f) for β-WCl_6.

positioned between 5 eV and 10 eV is estimated by 1.5 $\Omega^{-1}cm^{-1}$, 1.4 $\Omega^{-1}cm^{-1}$ and 1.7 $\Omega^{-1}cm^{-1}$ for β-WCl_6, α-WCl_6 and WCl_5. The real dielectric function helps in predicting the nonlinear optical behavior of the material. The imaginary part of the dielectric function represents the absorptive capacity of such material. We can observe that the imaginary component of the dielectric function attains non-zero magnitude at energy identical of that corresponding to the direct Γ→Γ band gap value. The intense peak of imaginary dielectric function is located at about 5 eV, which suggest inter band transition, and the photon emission is not possible in this material. The static dielectric function is 2.8, 4 and 8.8 for β-WCl_6, α-WCl_6 and WCl_5. The refractive index of the material measures its transparency to incident spectral radiation. The static refractive index is 2.8, 2.2 and 5.5 for β-WCl_6, α-WCl_6 and WCl_5 and reaches a maximum value of 5, 4 and 8.5 and describes the behavior of light in a medium. It is in agreement with the experimental obtained result of 1.88 [32]. The refractive index is more important when photons move through the material and when bonds between atoms are covalent. The maximum static refractive index is 3.5, 2.8 and 5.5 at 15 eV for β-WCl_6, α-WCl_6 and WCl_5. The static refractive index starts at energy identical of that corresponding to the direct band gap values.

4. Conclusion

We studied the cubic β-W_8, the trigonal WCl_3, the monoclinic WCl_4 and WCl_5, the hexagonal α-WCl_6 and β-WCl_6 and the orthorhombic Cl_2 structures. The monoclinic WCl_5 and the trigonal WCl_3 are the more stable phases. WCl_6 phase may be present in two crystal forms, such as the hexagonal (*P*-3 m1, 164) β-WCl_6 and the hexagonal (*R*-3, 148) α-WCl_6. The obtained bond distance in α-WCl_6 and β-WCl_6 are significantly longer than the mean bond distances in WCl_4 and WCl_5. There is a direct Γ-Γ band gap for WCl_3 (1.78 eV), WCl_5 (0.08 eV), β-WCl_6 (1.746 eV) and α-WCl_6 (1.803 eV), while WCl_4 has the metallic character. The atomic geometry of monoclinic WCl_4 and WCl_5 contain an ordered arrangement of W vacancies. The PDOS profile of W and Cl are similar throughout the whole energy region, indicating the presence of hybridization between W and Cl electrons. One shares the charge density at each point between atoms in proportion to the free atomic density, so that the distribution of bound and localized atoms resembles the molecular density. The atomic charges follow the expected chemical trends and are also similar to the Hirshfeld atomic charges. The absorption coefficient of β-WCl_6 and α-WCl_6 systems is 80000 cm^{-1} and 225000

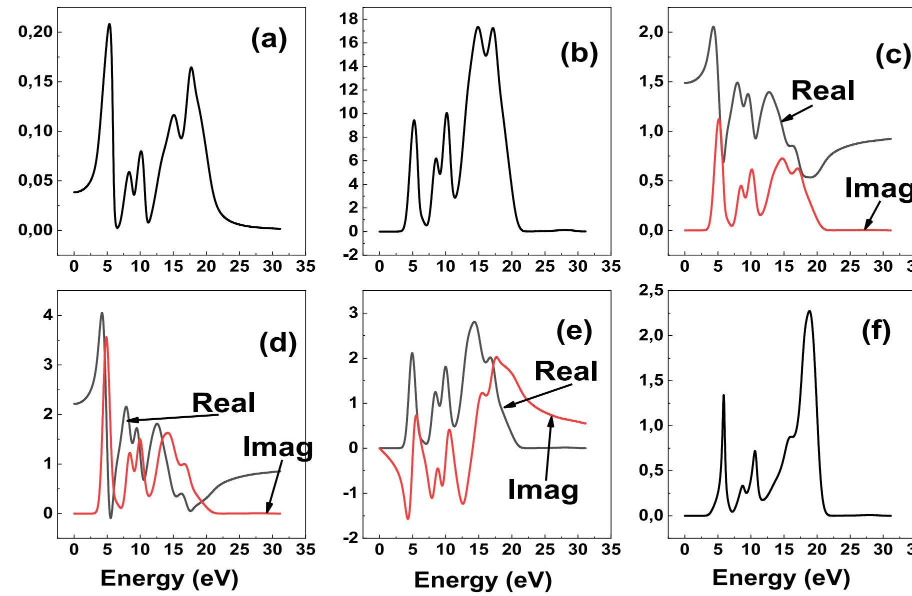

Fig. 7. The reflectivity (a), absorption (10^4 cm^{-1}) (b), conductivity (c), real and imaginary parts of dielectric function (d), refractive index (e) and loss function (f) for α-WCl_6.

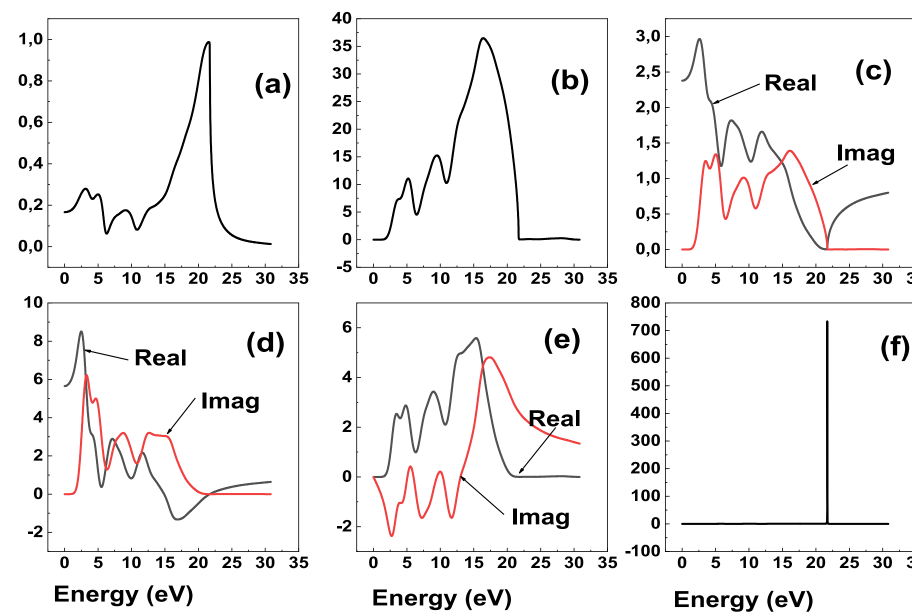

Fig. 8. The reflectivity (a), absorption (10^4 cm^{-1}) (b), conductivity (c), real and imaginary parts of dielectric function (d), refractive index (e) and loss function (f) for WCl_5.

cm^{-1} respectively, the band gap 1.746 eV and 1.803 eV, which are characteristic properties of a good absorber material.

CRediT authorship contribution statement

R. Boudissa: Formal analysis, Data curation. **Y. Madkour:** Software, Project administration. **T. Chihi:** Funding acquisition, Formal analysis. **M.A. Ghebouli:** Methodology, Investigation. **H. Bouandas:** Methodology, Investigation. **F. Benlakhdar:** Funding acquisition, Formal analysis. **M. Fatmi:** Writing – review & editing, Visualization, Validation. **B. Ghebouli:** Methodology, Investigation. **Munirah D. Albaqami:** . **Saikh Mohammad:** Investigation. **M. Habila:** Investigation. **M. Sillanpää:** Project administration.

Declaration of competing interest

The authors declare that they have no known competing financial interests or personal relationships that could have appeared to influence the work reported in this paper.

Data availability

The authors do not have permission to share data.

Acknowledgements

This work was funded by the Researchers Supporting Project Number (RSP2024R267) King Saud University, Riyadh, Saudi Arabia.

References

[1] G. Karkera, M. Soans, B. Dasari, E. Umeshbabu, M.A. Cambaz, Z. Meng, T. Diemant, M. Fichtner, Tungsten Oxytetrachloride as a positive electrode for Chloride-Ion Batteries, Energ. Technol. 10 (2022) 2200193.
[2] H. Okamoto H. Okamoto Phase Diagrams for Binary Alloys (ASM international Materials Park OH) 44 2000.
[3] B. Schimmelpfennig, U. Wahlgren, O. Gropen, A. Haaland, "The gas phase structures of tungsten chlorides: density functional theory calculations on WCl 6, WCl 5, WCl 4, WCl 3 and W 2 Cl 6,", J. Chemical SocietyDalton Trans. 1616–1620 (2001).
[4] B. Ivanova, Comment on "Comment on 'Crystallographic and theoretical study of the atypical distorted octahedral geometry of the metal chromophore of zinc (II) bis ((1R, 2R)-1, 2-diaminocyclohexane) dinitrate'", J. Mol. Struct. 1287 (2023) 135746.
[5] A. Sevy, R.F. Huffaker, M.D. Morse, Bond dissociation energies of tungsten molecules: WC, WSi, WS, WSe, and WCl, Chem. A Eur. J. 121 (2017) 9446–9457.
[6] L. Henry, V. Svitlyk, G. Garbarino, D. Sifre, M. Mezouar, Structure of solid chlorine at 1.45 GPa, Zeitschrift Für Kristallographie-Crystalline Materials 234 (2019) 277–280.
[7] W. Keesom, K. Taconis, On the crystal structure of chlorine, Physica 3 (1936) 237–242.
[8] R.L. Collin, The crystal structure of solid chlorine, Acta Crystallogr. 5 (1952) 431–432.
[9] N. Bartalucci, F. Marchetti, S. Zacchini, G. Pampaloni, Decarbonylation of phenylacetic acids by high valent transition metal halides, Dalton Trans. 48 (2019) 5725–5734.
[10] K. Rinke, H. Schäfer, Nachweis der moleküle W2Cl6 und W3Cl9 im gaszustand, Angew. Chem. 79 (1967) 650–651.
[11] K.-O. Kirk-Othmer, Encyclopedia of chemical technology, **2** Set, John Wiley & Sons, 2007.
[12] R.A. Lewis, Hawley's condensed chemical dictionary, John Wiley & Sons, 2016.
[13] R. Lemus, C.F. Venezia, An update to the toxicological profile for water-soluble and sparingly soluble tungsten substances, Crit. Rev. Toxicol. 45 (2015) 388–411.
[14] M. Bortoluzzi, F. Marchetti, M.G. Murrali, G. Pampaloni, S. Zacchini, The chlorinating behaviour of WCl 6 towards α-aminoacids, Dalton Trans. 44 (2015) 8729–8738.
[15] M. Bortoluzzi, F. Guarra, F. Marchetti, G. Pampaloni, S. Zacchini, Different outcomes in the reactions of WCl6 with carboxylic acids, Polyhedron 99 (2015) 141–146.
[16] J. t Taylor and P.-W. Wilson, "Neutron and X-ray powder diffraction studies of the structure of uranium hexachloride," Acta Crystallographica Section B: Structural Crystallography and Crystal Chemistry 30 1974 1481 1484.
[17] D. Smith, R. Landingham, G. Smith, Q. Johnson, The crystal structure of WCl6, Acta Crystallogr. Sect. B: Struct. Crystallogr. Cryst. Chem. 24 (1968) 1563.
[18] F.A. Cotton, C. Rice, Tungsten pentachloride, Acta Crystallogr. Sect. B: Struct. Crystallogr. Cryst. Chem. 34 (1978) 2833–2834.
[19] R. McCarley, T. Brown, The Preparation and reactions of some tungsten (II) and Tungsten (IV) Halides, Inorg. Chem. 3 (1964) 1232–1236.
[20] V. Kolesnichenko, D.C. Swenson, L. Messerle, Facile reduction of tungsten halides with nonconventional, mild reductants. I. Tungsten tetrachloride: several convenient solid-state syntheses, a solution synthesis of highly reactive (WCl4) x, and the molecular structure of polymeric tungsten tetrachloride, Inorg. Chem. 37 (1998) 3257–3262.
[21] Y. Zheng, E. Jonas, J. Nuss, H.G. von Schnering, The DMSO Solvated octahedro-[W6Cl] Cl Cluster Molecule, Z. Anorg. Allg. Chem. 624 (1998) 1400–1404.
[22] S.J. Clark, M.D. Segall, C.J. Pickard, P.J. Hasnip, M.I. Probert, K. Refson, M. C. Payne, First principles methods using CASTEP, Zeitschrift Für Kristallographie-Crystalline Materials 220 (2005) 567–570.
[23] T. Chihi, M. Fatmi, B. Ghebouli, First-principles prediction of metastable niobium and tantalium nitrides M4N5 and M5N6 stoichiometry, Solid State Sci. 14 (2012) 80–83.
[24] H.J. Monkhorst, J.D. Pack, Special points for Brillouin-zone integrations, Phys. Rev. B 13 (1976) 5188.
[25] P. Hohenberg, W. Kohn, Density functional theory (DFT), Phys. Rev 136 (1964) B864.
[26] W. Kohn, L.J. Sham, Self-consistent equations including exchange and correlation effects, Phys. Rev. 140 (1965) A1133.
[27] E.L. Albuquerque, U. Fulco, V. Freire, E. Caetano, M. Lyra, F. de Moura, DNA-based nanobiostructured devices: the role of quasiperiodicity and correlation effects, Phys. Rep. 535 (2014) 139–209.
[28] H.-J. Lunk, H. Hartl, Discovery, properties and applications of tungsten and its inorganic compounds, ChemTexts 5 (2019) 15.
[29] A. Nägele, J. Glaser, H. Meyer, "W6Cl18: Neue Synthesen, neue Strukturverfeinerung, elektronische Struktur und Magnetismus,"Zeitschrift für anorganische und allgemeine, Chemie 627 (2001) 244–249.
[30] Y.S. Ezhov, S. Komarov, Determination of the molecular constants of tungsten tetrachloride from electron diffraction data, J. Struct. Chem. 25 (1984) 71–76.
[31] Y.S. Ezhov, A. Sarvin, An electron diffraction study of tungsten pentachloride, J. Struct. Chem. 24 (1983) 140–143.
[32] G. Hautier, S.P. Ong, A. Jain, C.J. Moore, G. Ceder, Accuracy of density functional theory in predicting formation energies of ternary oxides from binary oxides and its implication on phase stability, Phys. Rev. B 85 (2012) 155208.